Electronic Supplementary Material (ESI) for Physical Chemistry Chemical Physics.

Electronic Supplementary Information

^{31}P Spin-lattice and singlet order relaxation mechanisms in pyrophosphate studied by isotopic substitution, field shuttling NMR, and molecular dynamics simulation

David E. Korenchan,†[1] Jiaqi Lu,†[1] Mohamed Sabba,[2] Laurynas Dagys,[2] Lynda J. Brown,[2] Malcolm H. Levitt,[2] and Alexej Jerschow*[1]

1. Department of Chemistry, New York University
100 Washington Square E, New York, NY 10003
Email: alexej.jerschow@nyu.edu

2. School of Chemistry, University of Southampton
Southampton SO17 1BJ, UK.

† These authors contributed equally.

Experimental Procedures

Chemicals

Deuterium oxide (D_2O, >99.96% atom % D) was purchased from Sigma (St. Louis, MO, USA). Sodium hydroxide (NaOH, ca. 85% purity) and potassium hydroxide (KOH, >99% purity) were purchased from Fisher Scientific (Hampton, NH, USA). Ethylenediamine tetraacetate (EDTA, disodium dihydrate) was purchased from Sigma. Phosphoric acid ($^{18}O_4$, ~80 wt. % in $H_2{}^{18}O$, 95 atom % ^{18}O) and silver nitrate (99.5% purity) were supplied by Merck. Dibenzyl phosphite (95% purity) was supplied by Acros Organics. All other solvents and reagents were used as received from standard chemical suppliers.

NMR sample preparation, degassing

The samples of the synthesized $^{18}O/^{16}O$ unsymmetric pyrophosphate (uPP_i) that were used for NMR experiments are described below. Note that the pD was determined using a conventional pH meter, calibrated with pH 7 and 10 calibration buffers, and then adding 0.4 to the reading on the meter[1]. All pH meter measurements were performed at room temperature. We took the highest pK_a of the pyrophosphate to be 9.4,[2] assuming that the pK_a does not change upon partial ^{18}O labeling. We then estimated the highest pyrophosphate pK_a in D_2O to be $pK_a(D_2O) = pK_a(H_2O) + 0.6 =$ 10.0, based upon pK_a values in a similar range[3].

Tetrasodium uPP_i in D_2O (referred hereafter as "Na_4^+-uPP_i only"): This consisted of 30 mM of the synthesized $^{18}O/^{16}O$ unsymmetric pyrophosphate, tetrasodium salt, dissolved in D_2O. The solution pD was not directly measured; however, a similar solution made with unlabeled PP_i and the same reagents otherwise gave a pD measurement of 10.94.

Tetrasodium uPP_i with EDTA in D_2O: This sample consisted of 30 mM of the synthesized $^{18}O/^{16}O$ unsymmetric pyrophosphate, tetrasodium salt, dissolved in D_2O with 10 mM of sodium EDTA added. The solution pD was not directly measured; however, a similar solution made with unlabeled PP_i and the same reagents otherwise gave a pD measurement of 10.29.

Tetrasodium uPP_i with KOH in D_2O: This sample consisted of 30 mM of the synthesized $^{18}O/^{16}O$ unsymmetric pyrophosphate, tetrasodium salt, dissolved in D_2O with about 10 equivalents of KOH added. The solution pD was not directly measured; however, a similar solution made with unlabeled PP_i and the same reagents otherwise gave a pD measurement of 14.4. This was the main NMR sample used in this study, relevant to the data displayed in Fig. S1 and 3 in the main text.

Additionally, the uPP_i sample with KOH added was degassed prior to some NMR experiments, according to the following protocol. 367 mg of the KOH sample described in the preceding paragraph had 108.5 mg D_2O added to it in order to compensate for D_2O loss during degassing. The sample solution was placed within a 5 mm NMR tube fitted with a J Young valve on top and attached to a custom-built degassing setup. The bottom half of the sample in the tube was carefully frozen in liquid nitrogen, and the tube was slowly opened to vacuum while gently warming the sides of the tube in order to help gas bubbles to escape. This freeze-vacuum cycle was repeated a total of 7 times, after which no gas bubbles were visible upon vacuum. Finally, the NMR tube was charged with 2 bar of argon gas and sealed.

NMR spectrometry and processing

All ^{31}P NMR spectroscopy was pulsed and detected at 9.4 T, with a total repetition time set to 5 times the uPP$_i$ ^{31}P T_1 value at this field strength. For each sample, the probe was tuned and matched prior to obtaining the 90° pulse length by determining the zero-crossing at a tip angle of 360° and dividing the resulting pulse length by four. The pulse-acquire ^{31}P NMR spectrum used for spectral fitting (Fig. 1, main text) was acquired with the following parameters: 1 s acquisition time, 61 ms dwell time, 8192 complex points, 8.2 kHz spectral width, 1 scan. The SLIC optimization and field-shuttling experiments to measure R_1 and R_S used the following acquisition parameters: 0.5 s acquisition time, 61 ms dwell time, 4096 complex points, 8.2 kHz spectral width. The inversion-recovery field-shuttling sequence for R_1 acquired 2 scans per timepoint; the SLIC field-shuttling sequence for R_S acquired 4 scans per timepoint. The optimizations for the SLIC sequence were run with 2 scans per point and included a delay of 50 ms between the first SLIC spin-lock pulse and the start of the T_{00} filter, which was included to eliminate all coherences except singlet order. The T_{00} filter parameters were the same as previously described[4].

The ^{31}P pulse-acquire spectrum used for spectral fitting (Fig. 1, main text) was zero-filled by a factor of 4 and phased within Topspin prior to being loaded into MATLAB. The homonuclear ^{31}P-^{31}P scalar coupling and ^{31}P chemical shift difference were determined by NMR spectral simulation performed using the Spinach MATLAB package (http://spindynamics.org/group/). The "fminunc" function within MATLAB was used to minimize the residual between simulated and experimental spectra. Residual minimization focused only on the four NMR peaks of the uPP$_i$ doublet of doublets; all other regions of the spectrum were excluded from the fitting routine.

The SLIC optimization and field-shuttling experimental data were processed entirely in MATLAB using custom scripts. For the SLIC optimization, data were zero-filled by a factor of 4, and the uPP$_i$ doublet of doublets was integrated in magnitude mode. The field-shuttling experiments were processed in bulk, in which the data were zero-filled by a factor of 4 and apodized by 5 Hz, the first timepoint of one inversion-recovery and one SLIC experiment were phased, and then the phasing parameters were applied to the other experiments acquired that day prior to integration in phased mode. Inversion-recovery data were fit to an equation of the form $y = A(1\text{-}2e^{-Bx}) + C$, and the SLIC data were fit to an equation of the form $y = Ae^{-Bx} + C$. Almost all data sets were fitted with $R^2 > 0.98$; the only exceptions were the R_S fit for the uPP$_i$-EDTA sample at 1 T ($R^2 = 0.959$) and 9.4 T ($R^2 = 0.886$), and the R_S fit for the uPP$_i$-KOH sample at 9.4 T ($R^2 = 0.871$).

The molecular uPP$_i$ translational diffusion coefficient was measured using the "stegp1s" pulse sequence in Topspin, which is a simulated-echo pulsed-field gradient sequence. The parameters used were the following: 1 s acquisition time, 61 ms dwell time, 8192 complex points, 8.2 kHz spectral width, 4 scans per field gradient amplitude, diffusion time D = 100 ms, gradient pulse duration δ = 7.5 ms, smoothed-square gradient pulses (SMSQ10.100) with a 1 ms delay for gradient recovery. The uPP$_i$ ^{31}P multiplet integral was integrated in phased mode at each gradient strength, and data were fitted in Topspin to an equation of the form $I = I_0\exp(-D(\gamma G_i\delta)^2(\Delta-\delta/3))$, where I is the integral, I_0 is the fitted integral with no diffusion gradients, γ is the ^{31}P gyromagnetic ratio, G_i is the gradient amplitude (which varies over the course of the experiment), and Δ and δ are the standard timing parameters in a diffusion measurement.

Theory

Derivation of spin rotation relaxation contributions: general formulation

Pileio[5] has provided very general relaxation expressions, and we derive here our spin-rotation relaxation expression of interest. The work by Pileio also provided a simplified expression for the regime of isotropic small-step rotational motion, which applies here. For that case, the starting point is Pileo's Eq. (46) in combination with the author's Table 1, which gives the relaxation superoperator for the spin-rotation interaction as:

$$\mathbf{\Gamma}^{\boldsymbol{SR,jk}} = -\frac{1}{2\hbar^2}\sum_{m=-1}^{1}(-1)^m \mathcal{J}_{l,m}^{j,k}(\omega)\boldsymbol{T}_{\boldsymbol{l,-m}}^{\boldsymbol{j}}\boldsymbol{T}_{\boldsymbol{l,m}}^{\boldsymbol{k}}. \tag{1}$$

The indices j and k denote the different spins, $\mathbf{T}_{l,m}$ are the spin commutation superoperators (given below) for the spin-rotation interaction of rank l and order m for spins j or k, and $\mathcal{J}_{l,m}^{j,k}$ is the spectral density function for the interaction. Note that the additional factor of $\hbar^2$ in the denominator arises from the conversion of energy units to angular frequency units in the Hamiltonians, so that the spin-rotation tensors can be represented in angular frequency units, as is common practice.

The commutation superoperators are to be understood to perform $\mathbf{T}_{l,m} = [T_{l,m}, \ldots]$ when acting on an operator, and the operators $T_{l,m}$ are given for the spin-rotation interaction as (see Table 1 of Pileio):

$T_{1,0}^{j} = I_z^j$

$T_{1,0}^{j} = \mp\frac{1}{\sqrt{2}} I_{\pm}^{j}.$

The spectral density function is given in terms of the correlation functions $G_{llmm}^{j,k}$ in analogy to Pileio's Eq. (45) as follows:

$$\mathcal{J}_{l,m}^{j,k}(\omega) = 2\int_0^{\infty} G_{llmm}^{j,k}(\tau)\exp(-i|m|\omega\tau)\,d\tau. \tag{2}$$

For the case of small overall molecular reorientation (compared to the change of local angular momentum), the correlation function is given according to Pileio's Eq. (56) as

$$G_{11,mm}^{j,k}(\tau) = \frac{1}{3}\sum_{p}\overline{A_{1p}^{j}(t)A_{1p}^{k*}(t+\tau)}, \tag{3}$$

where the spatial tensor components A_{1p} are given in terms of the spin rotation tensor (C) and the angular momentum (J) components in their principal axis frame as follows (Pileio, Table 1):

$$A_{10}^{j}(t) \;=\; C_{zz}^{j}J_z^j(t) \tag{4}$$

$$A_{1\pm1}^{j}(t) \;=\; \mp\frac{1}{\sqrt{2}}(C_{xx}^{j}J_x^j(t) \pm iC_{yy}^{j}J_y^j(t)). \tag{5}$$

We assume here the time dependence to arise mainly from the angular momentum.

Derivation of spin rotation relaxation contributions: spin-lattice relaxation

Since we consider only the rotation of the $-PO_3^-$ moiety about a single axis, we only need to perform the calculation of the correlation function for one component of the spatial tensors. This component is given the designation ∥ to indicate its orientation parallel to the rotation axis. For this case, we obtain

$$G_{11,mm}^{j,j}(\tau) = \frac{1}{3}\left(C_{\parallel}^{j}\right)^2 \overline{J_{\parallel}^{j}(t) J_{\parallel}^{j*}(t+\tau)}. \tag{6}$$

Converting from angular momentum to angular frequency of the rotation $\omega_{\parallel}^{j}$, we obtain

$$G_{11,mm}^{j,j}(\tau) = \frac{1}{3}\left(C_{\parallel}^{j} I_{\parallel}^{j}\right)^2 \overline{\omega_{\parallel}^{j}(0)\omega_{\parallel}^{j}(\tau)}, \tag{7}$$

Where $I_{\parallel}^{j}$ is the moment of inertia of the rotating entity. In the last step we also assumed that the moment of inertia and the spin-rotation tensor component remain constant, and that ergodicity prevails in the averaging.

To calculate R_1^{SR} we apply the superoperator to the Zeeman term I_z, and calculate the observable $\langle I_z \rangle = Tr\{I_z \Gamma^{SR} I_z\}/Tr\{I_z I_z\}$. For this calculation, we drop the *j* superscript, as only a single spin is required here. Combining Eqs. (1) and (7) and the tensor definitions, we obtain

$$R_1^{SR} = \frac{2}{3\hbar^2} I_{\parallel}^2 C_{\parallel}^2 \overline{\omega_{\parallel}(0)\omega_{\parallel}(\tau)} = \frac{2}{3\hbar^2} I_{\parallel}^2 C_{\parallel}^2 \overline{\omega_{\parallel}(0)^2}\tau_J, \tag{8}$$

where in the last step we have used the fast motion regime expression, and τ_J is the correlation time of the rotation motion.

A consistency check can be performed here to compare this expression with the one often encountered in other literature, as follows.

Starting from McClung's[6] Eq. (22) we consider rotation only around the bridging PO bond, and so there is only one component in that equation,

$$R_1^{SR} = \frac{2k_B T}{3\hbar^2} I_{\parallel} C_{\parallel}^2 \tau_J. \tag{9}$$

Note that in this equation we have an estimate of the correlation function for the angular momentum incorporated (McClung's Eq. (17)). We can however calculate the correlation time for the angular velocity directly from MD and use it in this equation. To do so, we can use the expression for the average energy of the rotation (see, for example, Spiess[7] Eq. (4.83))

$$I\langle \omega^2 \rangle = k_B T \tag{10}$$

Inserting this for $k_B T$ into Eq. (9) above, we obtain

$$R_1^{SR} = \frac{2}{3\hbar^2} I_{\parallel}^2 C_{\parallel}^2 \overline{\omega_{\parallel}(0)^2}\tau_J, \tag{11}$$

which is equivalent to Eq. (8).

Derivation of spin rotation relaxation contributions: singlet order relaxation

To calculate the singlet order rate constant due to spin-rotation R_{SO}^{SR} we apply the superoperator to the SO term $\boldsymbol{I}^j \cdot \boldsymbol{I}^k$, and calculate the observable

$$\langle \boldsymbol{I}^j \cdot \boldsymbol{I}^k \rangle = Tr\{\boldsymbol{I}^j \cdot \boldsymbol{I}^k \boldsymbol{\Gamma}^{\boldsymbol{SR,j,k}} \boldsymbol{I}^j \cdot \boldsymbol{I}^k\} / Tr\{(\boldsymbol{I}^j \cdot \boldsymbol{I}^k)(\boldsymbol{I}^j \cdot \boldsymbol{I}^k)\}.$$

Combining Eqs. (1), (7) and the tensor definitions, and evaluating the double commutators, one obtains by following the same procedure as above

$$R_S^{SR,j,k} = \frac{2}{3\hbar^2}(C_\parallel I_\parallel)^2 \left(\overline{\omega_\parallel^j(0)^2} + \overline{\omega_\parallel^k(0)^2} - 2\kappa\overline{\omega_\parallel^j(0)\omega_\parallel^{k*}(0)}\right)\tau_J, \quad (12)$$

where κ is the correlation coefficient arising from the different spin-rotation tensor orientations. Combining the correlation coefficient between the tensors and the angular frequencies into the factor α, and recognizing the statistical equivalence between averages over j and k angular frequencies, we can write

$$R_S^{SR,j,k} = \frac{2}{3\hbar^2}(C_\parallel I_\parallel)^2 \left[2\overline{\omega_\parallel^j(0)^2}(1-\alpha)\right]. \quad (13)$$

This expression is similar to the one provided in Ref. 8 for the paramagnetic mechanism. A correlation factor α of 0 indicates complete independence of the processes on the two phosphorus atoms, and the SO relaxation rate constant is then double the R_1 constant. Full correlation ($\alpha = 1$) would mean that the interaction is inactive for SO. Complete anticorrelation ($\alpha = -1$) leads to SO relaxation being a quadruple of R_1 relaxation.

Results and Discussion

Fig. S1 compares the ^{31}P NMR spectra, R_1 and R_S curves between the three uPP$_i$ samples: uPP$_i$ only, uPP$_i$ with EDTA, and uPP$_i$ with KOH. Adding either EDTA or KOH to the uPP$_i$ in solution drastically reduces the linewidth and lengthens R_1 and R_S. A thorough investigation into these mechanisms is beyond the scope of the present work. A few studies have demonstrated that EDTA can lengthen phosphate ^{31}P T_1 and T_2 relaxation time constants in the presence of metal cations such as Fe^{3+},[9] Cu^{2+},[10] and Mg^{2+}.[11] However, these effects are strongly pH-dependent[10, 11], and EDTA can even accentuate line broadening at lower pH values[11]. Additionally, two separate samples of unlabeled PP$_i$, one prepared with 10 eq NaOH and one compared with 10 eq KOH, had T_1 measurements at 9.4 T of 8.70 s and 9.37 s, respectively.

Fig. S2 displays the results of pulse sequence optimization for the SLIC spin-lock pulses used for the study. Although the pulse nutation frequency was not optimized on the KOH sample (Fig. S2B), it was assumed that the uPP$_i$ J_{PP} coupling and therefore the optimal nutation frequency would not change with the sample conditions. The data in Fig. S2B were fit to a curve of the form $y = A + B\sin^4(\pi Cx/\sqrt{2})$ in order to obtain the pulse length corresponding with the maximum signal[12]. As reported in the main text, the optimal spin-lock SLIC pulses for the KOH sample corresponded with a homonuclear ^{31}P-^{31}P J-coupling of 20.3 Hz and a chemical shift difference of 12.3 Hz.

Fig. S3 visualizes the spin-rotation tensor components as determined using Gaussian. The simulation details and spin-rotation tensor component values are reported in the main text.

Fig. S4 shows field cycling measurement results for R_1 and R_S on two samples: the uPP_i-EDTA sample and the uPP_i-KOH sample following degassing. Both samples gave results that were very similar to those reported for the non-degassed uPP_i-KOH sample in Fig. 3 of the main text.

Fig. S5 shows the synthesis of $^{18}O/^{16}O$ unsymmetrical pyrophosphate tetrasodium salt 6, henceforth referred to as uPPi.

Fig. S6 shows the calculated Frobenius norms and eigenvalues of the symmetric and antisymmetric components of the chemical shift anisotropy (CSA) tensors, for individual snapshots from the molecular dynamics simulations.

Fig. S7 shows the results of a pulsed-field gradient diffusion NMR experiment used to measure the uPP_i translational diffusion coefficient, D. The diffusion coefficient was determined from the fitted curve to be $0.37 \cdot 10^{-9}$ m^2/s. This was significantly larger than the translation diffusion coefficient determined from molecular dynamics simulations as $0.215 \cdot 10^{-9}$ m^2/s, which used simulation conditions of 300 K temperature with water as the solvent. As mentioned in the main text, simulated correlation times were adjusted by the ratio of experimental to simulated diffusion coefficients in order to better match the viscosity and motional regime conditions between experiment and simulation.

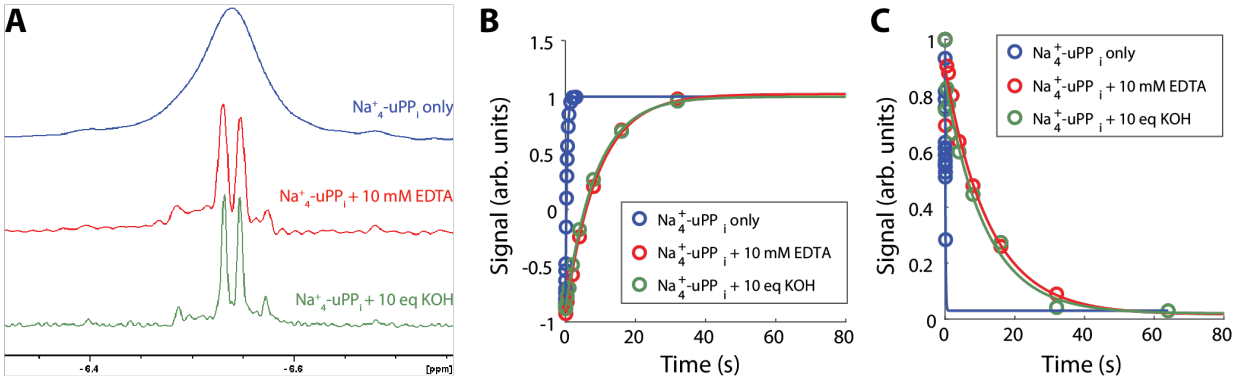

Fig. S1. Comparison of $^{18}O/^{16}O$ unsymmetric pyrophosphate sample preparations mentioned in the Experimental Procedures above. (**A**) Conventional ^{31}P NMR spectra of the three sample preparations, obtained at 9.4 T. (**B-C**) Recovery/decay curves obtained from ^{31}P NMR at 9.4 T of the three sample preparations using (**B**) a T_1 inversion-recovery sequence; and (**C**) a SLIC singlet order sequence.

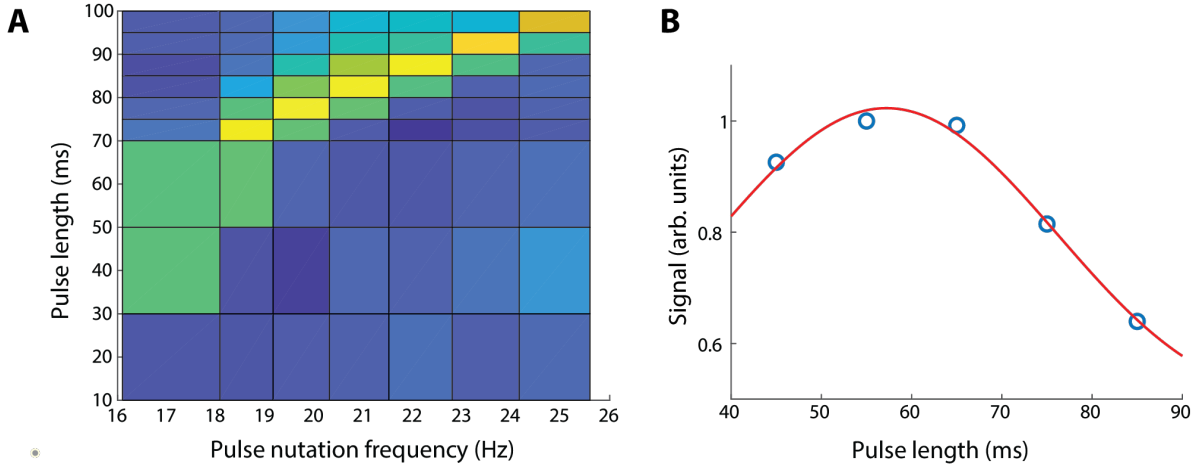

Fig. S2. Optimization of uPP$_i$ ^{31}P singlet-triplet conversion using the SLIC pulse sequence at 9.4 T. (**A**) Plot of singlet-derived NMR signal as a function of SLIC spin-lock pulse length and nutation frequency, performed on the uPP$_i$-EDTA sample. The maximum signal corresponded with a pulse length of 80 ms and a nutation frequency of 20.3 Hz. (**B**) Plot of singlet-derived NMR signal as a function of SLIC spin-lock pulse length, with a nutation frequency of 20.3 Hz, on the uPP$_i$-KOH sample. The data were fit to a curve of the form $\sin^4(x)$ to determine the maximum to be at a pulse length of 57.3 ms.

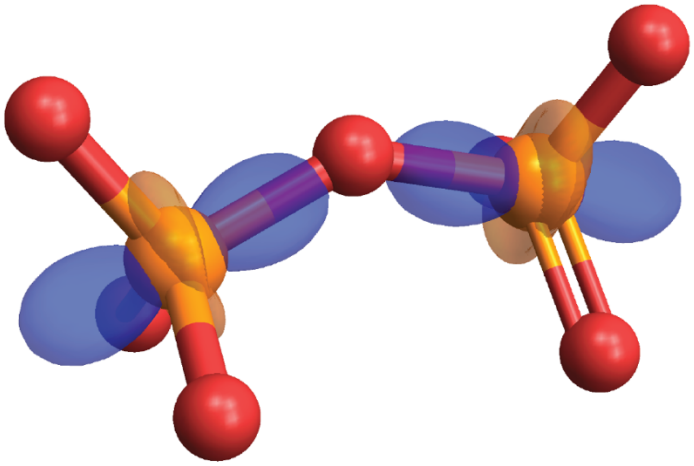

Fig. S3. Visualization of parallel and perpendicular spin-rotation tensor components in the molecular frame.

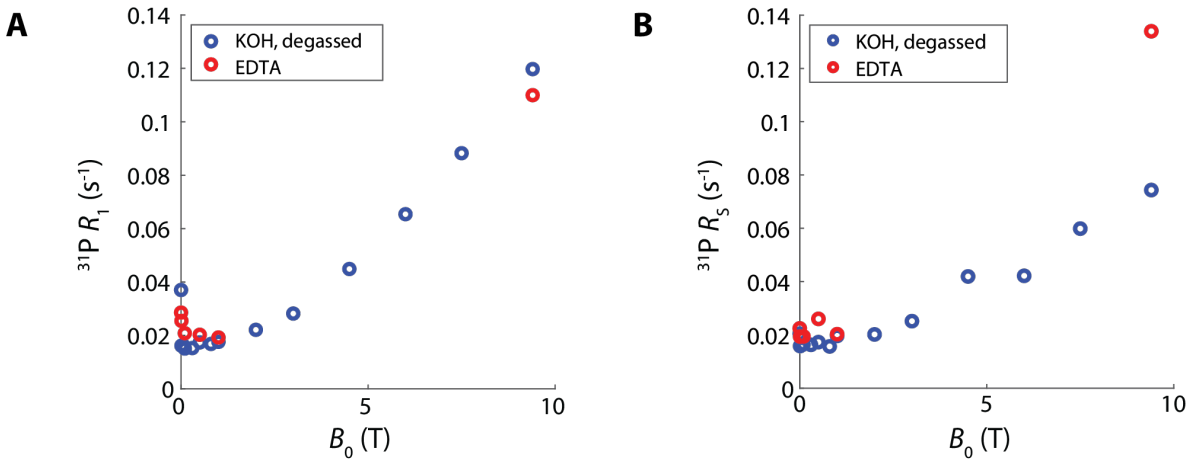

Fig. S4. Field-shuttling NMR measurements of R_1 and R_S under sample preparation conditions different from those reported in Fig. 3 of the main text. (**A**) R_1 measurements via inversion-recovery; (**B**) R_S measurements via the SLIC sequence.

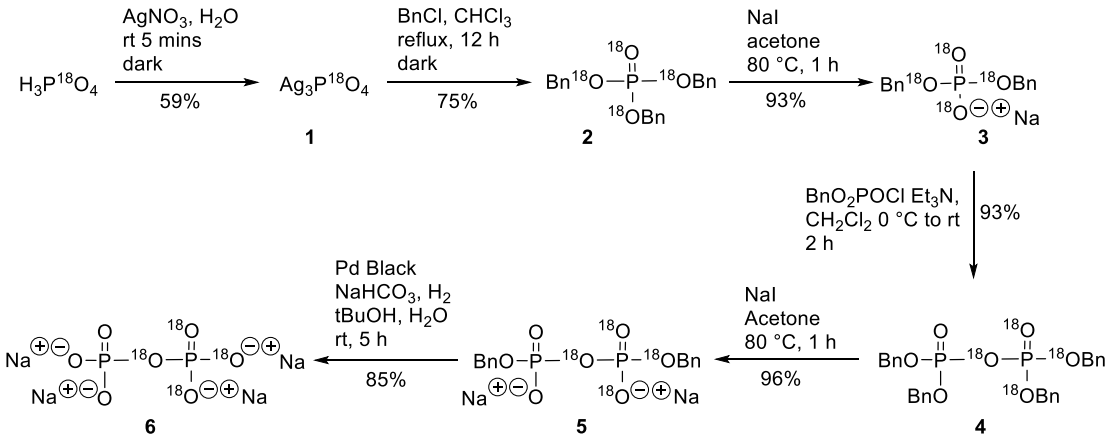

Fig. S5. Synthesis of $^{18}O/^{16}O$ unsymmetrical pyrophosphate tetrasodium salt **6**.

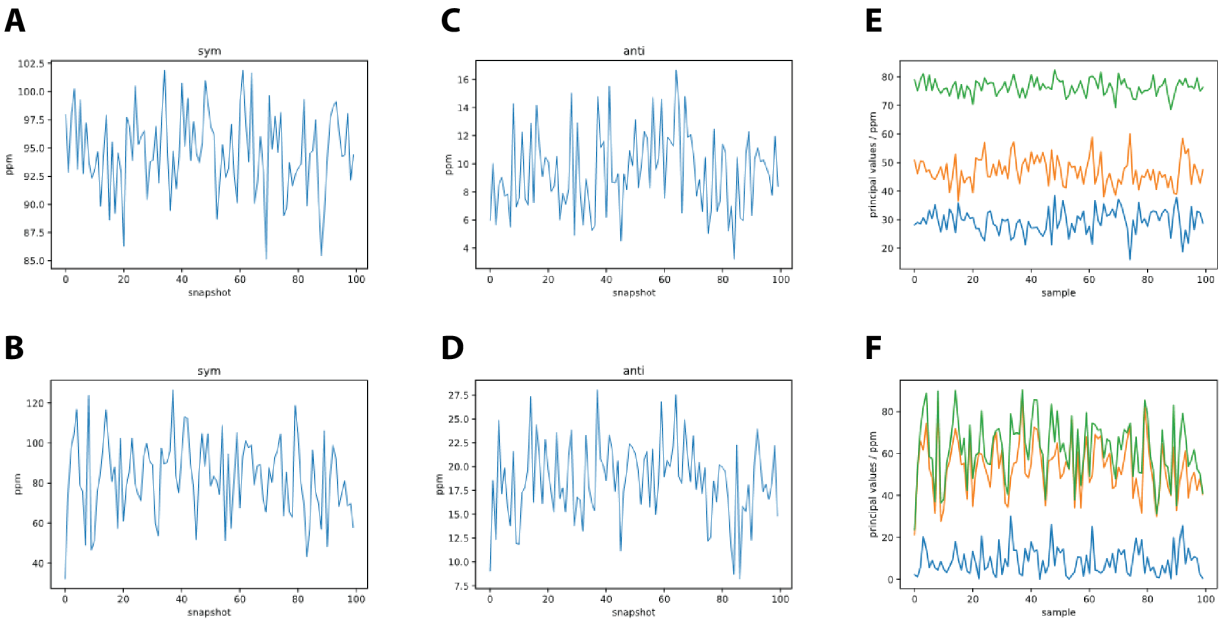

Fig. S6. Calculated CSA parameters of snapshot configurations extracted from molecular dynamics simulations of the uPP$_i$ molecule (100 snapshots). (**A-D**) Frobenius norms of (**A**) the symmetric component of the individual CSA tensor; (**B**) the symmetric component of the difference tensor between CSA tensors; (**C**) the antisymmetric component of the individual averaged CSA tensor; (**D**) the antisymmetric component of the difference tensor between CSA tensors; (**E-F**) Eigenvalues of the symmetric components of (**E**) individual CSA tensors; and (**F**) difference tensor between CSA tensors.

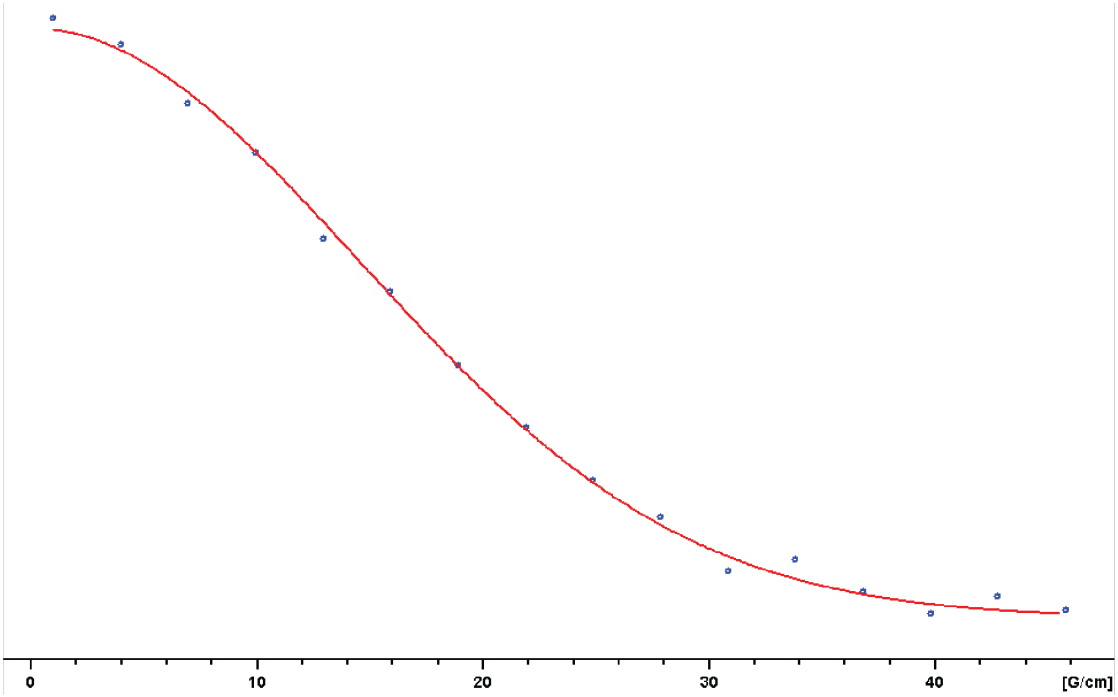

Fig. S7. Plot of ^{31}P signal intensity as a function of gradient strength during a pulsed-field gradient NMR diffusion experiment. Data are fitted to a curve of the type $I = I_0\exp(-D(\gamma G_i\delta)^2(\Delta-\delta/3))$ to obtain a uPP_i translational diffusion coefficient of $0.37\cdot10^{-9}$ m^2/s.

Reference

1. Mikkelsen, K. and S.O. Nielsen, *Acidity Measurements with the Glass Electrode in H2O-D2O Mixtures.* Journal of Physical Chemistry, 1960. **64**(5): p. 632-637.
2. McElroy, W.D. and B. Glass, *Phosphorus metabolism : a symposium on the role of phosphorus in the metabolism of plants and animals. Vol. I*. 1951. 1 vol. (XVI-762 p.).
3. Mora-Diez, N., et al., *Theoretical study of deuterium isotope effects on acid-base equilibria under ambient and hydrothermal conditions.* Rsc Advances, 2015. **5**(12): p. 9097-9109.
4. Tayler, M.C. and M.H. Levitt, *Accessing long-lived nuclear spin order by isotope-induced symmetry breaking.* J Am Chem Soc, 2013. **135**(6): p. 2120-3.
5. Thomas, E.L., et al., *Whole body fat: content and distribution.* Progress in nuclear magnetic resonance spectroscopy, 2013. **73**: p. 56-80.
6. McClung, R., *Spin–Rotation Relaxation Theory*. 2007.
7. Spiess, H.W., *Rotation of molecules and nuclear spin relaxation*, in *Dynamic NMR spectroscopy*. 1978, Springer. p. 55-214.
8. Tayler, M.C. and M.H. Levitt, *Paramagnetic relaxation of nuclear singlet states.* Physical Chemistry Chemical Physics, 2011. **13**(20): p. 9128-9130.
9. Elgavish, G.A. and J. Granot, *Enhancement of P-31 Relaxation Rates of Ortho-Phosphate and of Atp in the Presence of Edta - Evidence for Edta-Fe3+-Phosphate Ternary Complexes.* Journal of Magnetic Resonance, 1979. **36**(1): p. 147-150.
10. Granot, J., G.A. Elgavish, and J.S. Cohen, *P-31 Relaxation-Times of Inorganic-Phosphate and Nucleotides in Aqueous-Solution.* Journal of Magnetic Resonance, 1979. **33**(3): p. 569-575.
11. Bass, M.B. and H.J. Fromm, *Trans-1,2-Diaminocyclohexane-N,N,N',N'-Tetraacetic Acid Is Superior to Ethylenediamine-N,N,N',N'-Tetraacetic Acid for Sequestering Mg-2+ in P-31 Nmr Experiments Involving Atp Spectra at Neutral and Acidic Ph.* Analytical Biochemistry, 1985. **145**(2): p. 292-301.
12. DeVience, S.J., R.L. Walsworth, and M.S. Rosen, *Preparation of nuclear spin singlet states using spin-lock induced crossing.* Phys Rev Lett, 2013. **111**(17): p. 173002.